Einstein–Bose Condensation of Onsager Vortices

Rahil N. Valani[1,2], Andrew J. Groszek[1], Tapio P. Simula[1]
[1] *School of Physics and Astronomy, Monash University, Victoria 3800, Australia and*
[2] *Department of Mechanical and Aerospace Engineering, Monash University, Victoria 3800, Australia*

We have studied statistical mechanics of a gas of vortices in two dimensions. We draw a sharp distinction between clustering and condensation of vortices and use these observables to show that the large scale vortex structures characteristic of two-dimensional turbulence emerge well before the critical temperature for the Einstein–Bose condensation transition of Onsager vortices is reached.

arXiv:1612.02930v1 [cond-mat.quant-gas] 9 Dec 2016

Perhaps the most astonishing aspect of turbulence is not the complexity of its dynamics but rather that it feeds the emergence of ordered structures out of chaos. The ubiquity of large eddies in two-dimensional fluid flows was also noted by Onsager who suggested that it might be possible to obtain a statistical mechanics description of hydrodynamic turbulence of two-dimensional flows based on discrete collections of point-like vortex particles [1]. In particular, Onsager predicted that turbulent two-dimensional systems could support large scale clustered vortex structures, later coined Onsager vortices, and that such structures would correspond to absolute negative temperature states of the vortex degrees of freedom [2]. Notwithstanding the negative absolute Boltzmann temperature states were observed in nuclear spin systems [3, 4] soon after Onsager's theoretical prediction, and more recently in the motional degrees of freedom of cold atoms confined in optical lattices [5], the negative temperature Onsager vortex states are yet to be uncovered in their original context of two-dimensional (super)fluid turbulence.

Kraichnan developed the theory of two-dimensional turbulence further, conjecturing that a scale invariant inverse energy cascade mechanism of incompressible kinetic energy could dynamically lead to the formation of Onsager vortices and even to their condensation and that: *"The phenomenon is analogous to the Einstein–Bose condensation of a finite two-dimensional quantum gas"* [6]. In the Kraichnan model the system scale Onsager vortex clusters would emerge due to a termination of the inverse cascade that accumulates energy at ever larger spatial scales. Ultimately, such a process could potentially lead to the Einstein–Bose condensation (EBC) of the Onsager vortices, which correspond to the highest accessible energy states of the vortices. In a neutral system with $N_{\rm tot}$ vortices in total the EBC of Onsager vortices occurs at a critical negative temperature $T_{\rm EBC} = -\alpha N_{\rm tot}/4$ [7–9], where $\alpha = \rho_s\kappa^2/4\pi k_B = T_{\rm HH}$ is the critical positive temperature for the Hauge–Hemmer pair-collapse transition [10, 11], which in the case of non-zero vortex core size becomes renormalised to the Berezinskii–Kosterlitz–Thouless (BKT) critical temperature $T_{\rm BKT} = T_{\rm HH}/2$ [12–14]. Here $k_{\rm B}$ is the Boltzmann constant, ρ_s is the (super)fluid density and $\kappa = h/m$ is the circulation quantum with h the Planck's constant and m the particle mass. However, despite the ubiquity of the large scale vortex structures in real two-dimensional fluid flows, search for experimental evidence for the existence of Einstein–Bose condensation of such structures continues.

The recent developments of imaging and manipulating compressible superfluids has sparked renewed interest in Onsager's statistical hydrodynamics theory of turbulence. Experiments employing harmonically trapped Bose-Einstein condensates of atoms have ranged from studies of dynamics of vortex dipoles [15] or few vortices [16] to three- [17] and two-dimensional [18–21] quantum turbulence. Moreover, uniform atom traps are becoming increasingly popular [22–27] and will be particularly useful for studies of quantum turbulence. This is partly because well defined trap walls enhance the vortex clustering signal in comparison to harmonically trapped systems [9, 19, 28, 29]. In the latter case, strong clustering has not been observed although in both cases Onsager vortices in decaying two-dimensional quantum turbulence has been predicted to emerge via an evaporative heating mechanism of vortices [9, 28].

The successes of the recent experimental developments have also spawned novel theoretical investigations [9, 28–36]. In addition to visual inspection, the presence of Onsager vortices has been associated with indicators such as the vortex dipole moment [9, 28], vortex clustering measures [30, 31, 34], or a peak in the power spectral density of incompressible kinetic energy [9, 32, 37]. However, a measurable that would distinguish between vortex clustering and their condensation has been lacking. Here we use *a vortex–particle duality* to define an EBC fraction that enables quantitative measurements of condensation of Onsager vortices in these two-dimensional systems. We have implemented a vortex classification algorithm [38] based on the prescription by Reeves *et al.* [31] and show that this classification can be used to distinguish between clustering and condensation of vortices and thereby uniquely identify the EBC of Onsager vortices. We find that the EBC fraction exhibits universal behavior independent of the number of vortices in the bounded circular system and that strong vortex clustering is prevalent already at temperatures far from the EBC transition. Such vortex clustering is a precursor to the EBC of Onsager vortices and is reminiscent of the quasi-condensation that precedes the superfluid phase transitions in low-dimensional quantum gas systems [39–42]. We postulate that neither an inverse energy cascade or a spontaneous evaporative vortex heating mechanism may supply a sufficient amount of incompressible kinetic

energy in these systems to induce the EBC transition, prompting a search for new ways to achieve the negative temperature EBC phase transition experimentally.

We consider $N_{\rm tot}$ singly quantised point-like vortices with a hard core of radius ξ and equal numbers of clockwise and counter-clockwise circulations confined in a circular disk of radius $R_\circ$, unless stated otherwise. The pseudo-Hamiltonian describing our system is [9, 43]:

$$H = \alpha k_{\rm B}\sum_j s_j^2 \log(1-r_j^2) - \alpha k_{\rm B}\sum_{i<j} s_i s_j \log(r_{ij}^2) \quad (1)$$
$$+\alpha k_{\rm B}\sum_{i<j} s_i s_j \log(1-2x_ix_j-2y_iy_j+r_i^2r_j^2),$$

where $r_j^2 = x_j^2 + y_j^2$ and x_j and y_j are the dimensionless Cartesian coordinates of the jth vortex measured in units of the system radius $R_\circ$ and $s_j = \pm 1$ determines the circulation direction of the jth vortex. The first, single-vortex, logarithmic term is due to the interaction of each vortex with its own image, the second represents the pairwise two-dimensional Coulomb-like interaction between ith and jth vortex separated by distance r_{ij} and the last term, due to the circular boundary, represents the interaction of system vortices with the images of all other vortices.

The dynamics of the point-like vortices are determined by the equations of motion [1]

$$\frac{\partial x_j}{\partial t} = \frac{\partial H}{\partial y_j} \quad \text{and} \quad \frac{\partial y_j}{\partial t} = -\frac{\partial H}{\partial x_j}. \quad (2)$$

To draw a closer correspondence with Hamiltonian mechanics, we may assign for each vortex a canonical coordinate $q_j = R_\circ x_j$ and momentum $p_j = -\beta R_\circ y_j$, where the unspecified constant β has the dimensions of mass times frequency. Thus the set of vortex coordinates $\{x_j, y_j\}$ in the real space are mapped onto points in the phase space $\{q_j, p_j\}$ spanned by the canonical conjugate variables. In this Hamiltonian analog the vortex particles move in one-dimensional real space tracing out orbits in the two-dimensional phase space, which is bounded by the circular wall of radius $R_\circ$. Equation (2) establishes the *vortex–particle duality*—that a vortex in a two-dimensional fluid may behave as a particle in a one-dimensional space. Hence, in contrast to Kraichnan's conjecture, we anticipate the EBC of Onsager vortices to be *analogous to the Bose–Einstein condensation of a finite one-dimensional quantum gas*. By ignoring the vortex–vortex interactions we obtain an ideal-gas model of vortex particles. A Maclaurin series expansion of the single vortex term in Eq. (1) with respect to r_j formally yields a one-dimensional harmonic oscillator Hamiltonian

$$H_0 = \alpha k_{\rm B}\sum_j s_j^2 \log(1-r_j^2) \approx -\frac{\alpha k_{\rm B}}{R_\circ^2\beta^2}\sum_j (p_j^2+\beta^2 q_j^2) \quad (3)$$

with an inverted energy spectrum with respect to the canonical case. Within the harmonic approximation, a single vortex v of this system will travel along a periodic phase space orbit $\{q_v, p_v\} = \{R_v\cos(\omega_v t), -\beta R_v \sin(\omega_v t)\}$, with orbital angular frequency ω_v and semi-axis R_v.

The Einstein–Brillouin–Keller semiclassical quantisation rule [44]

$$\oint p_v dq_v = \left(n + \frac{k}{4}\right) h, \quad (4)$$

where n is the principal quantum number and k is the Keller–Maslov index then evaluates to

$$\int_0^T p_v dq_v = \int_0^{\frac{2\pi}{\omega_v}} \omega_v \beta R_v^2 \sin^2(\omega_v t) dt = \pi\beta R_v^2, \quad (5)$$

where we have integrated over one period, $T = 2\pi/\omega_v$, of the vortex orbit. The one-dimensional oscillatory motion has two classical turning points, $k = 2$, and therefore the quantisation rule, the combination of Eqs (4) and (5), yields the energy spectrum $E_n = (n+\frac{1}{2})\hbar\omega_0 = \frac{1}{2}\beta\omega_0 R_v^2$. This implies a minimum semi-axis $\min(R_v) = \xi$ for the vortex trajectories and yields the zero-point energy $E_0 = \frac{1}{2}\beta\omega_0\xi^2$. In correspondence with the Heisenberg uncertainly relation, $\Delta q \Delta p \gtrsim \hbar/2$, the zero-point energy carries the information that the area A of the phase space is quantised in units of $\hbar = \beta\xi^2$. This reflects the fact that it is not possible to localize the position of the vortex inside an area smaller than the vortex core. By introducing an effective vortex mass $m_v = \hbar^2 R_\circ^2/2\alpha k_{\rm B}\xi^4$ and an oscillator frequency $\omega_0 = 2\alpha k_{\rm B}\xi^2/\hbar R_\circ^2$ in Eq. (3), the ideal-vortex Hamiltonian can be mapped directly onto a one-dimensional harmonically trapped ideal Bose gas model. All thermodynamical quantities immediately follow from such a mapping, for example, the positive critical temperature is approximately $T_{\rm BEC}^{1D} = N^{\rm atom}\hbar\omega_{1D}/k_{\rm B}\log(2N^{\rm atom})$ [45]. Using the vortex-particle duality, this translates to $T_{\rm EBC}^{\rm ideal} = -N^{\rm vortex}2\alpha\xi^2/R_\circ^2\log(2N^{\rm vortex})$. Comparison with the EBC critical temperature $T_{\rm EBC} = -N^{\rm vortex}\alpha/2$ of the interacting maximally charged one vortex species system shows that the vortex–vortex interactions have the effect of removing the dependence of the critical temperature on the details of the vortex core structure [46].

The BEC condensate fraction of a one-dimensional harmonically trapped ideal Bose gas is of particular interest and has the well known functional form $N_0^{\rm atom}/N^{\rm atom} = 1-(T/T_{\rm BEC})$, ignoring the logarithmic corrections [45, 47]. Analogously, we anticipate Einstein–Bose condensation of Onsager vortices when the phase space density $n_v\lambda_v \gtrsim 1$. Here n_v is the mean vortex density and $\lambda_v = h/\langle p\rangle \sim 2\pi\xi^2/\langle R_v\rangle$ is the thermal vortex de-Broglie wavelength, which in the vortex dual is inversely proportional to the size of an average temperature-dependent vortex orbit in the phase space. For N^* vortices confined within length $2R^*$ the EBC criterion becomes $\pi N^*\xi^2/\langle R_v\rangle R^* \sim 1$, which shows that condensation is expected when the vortices concentrate into a phase-space cluster with size of the order of $\sqrt{N^*}\xi$. In words, the EBC may form when the cores of the vortices begin to overlap. The situation bears resemblance

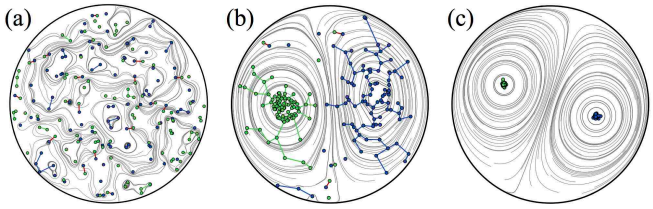

FIG. 1. (color online) Representative neutral vortex configurations (a)-(c) at respective temperatures $T/T_{\rm EBC} = 10^6, 1.022$, and 0.778, with $T_{\rm EBC} = -0.25\alpha N_{\rm tot}$ and $N_{\rm tot} = 200$. Vortices in vortex and antivortex clusters are connected by blue and green lines, respectively, vortex-antivortex dipoles are connected by red lines and free vortices are marked by isolated filled circles [38]. The streamlines illustrate the velocity field generated by the collection of vortices.

to rapidly rotating neutral superfluids, which are anticipated to successively condense into the various quantum-Hall-like states when the vortex cores begin to significantly overlap and the filling factor, or the number of fluid particles per vortex, approaches unity [48, 49].

These considerations lead us to define an Einstein–Bose condensate fraction of vortices as the ratio, N_0/N, of N_0 vortices of a given sign in a single many-vortex state to the total number of vortices N of that same sign in the system. The highest density of vortices is found within clusters and by denoting N^* to be the number of vortices in the largest cluster and $A^0 = N^*\beta\xi^2$ and A^* to be, respectively, the minimum possible phase space area occupied by the N^* vortices and the phase space area actually covered by them, we obtain

$$\text{EBC fraction} = \frac{N_0}{N} = \frac{N^*}{N}\frac{A^0}{A^*} = \frac{N^*}{N}\frac{\xi^2}{\langle r_{\rm nn}\rangle^2}. \qquad (6)$$

Thus the EBC fraction is the product of the largest cluster fraction N^*/N and the square of the ratio of single vortex core radius ξ to the mean intervortex spacing $\langle r_{\rm nn}\rangle$ within the cluster.

To study the thermodynamics of the Einstein–Bose condensation of Onsager vortices, we have performed Monte Carlo calculations using a Metropolis algorithm to find the equilibrium vortex configurations as functions of temperature for systems with $10, 20, 50, 100, 200, 300$ and 400 vortices [8, 9]. A hard core radius of $\xi = 0.001\ R_\circ$ was imposed on each vortex. The Monte Carlo samplings were performed for temperature in the range $T \in (-\infty, -0)$ with 10^6 microstates at each temperature after initial burn in of 10^6 steps. Out of the 10^6 microstates, 1000 uniformly spaced configurations were recorded and used for vortex classification analysis [38].

Figure 1 shows typical vortex configurations of disordered and clustered neutral vortex states of $N_{\rm tot} = 200$ vortices obtained from the Monte Carlo calculations at different temperatures. The same sign clusters, dipoles and free vortices are identified using a vortex classification algorithm [38] and the velocity field stream lines are included to visualise the superflow around the vortices.

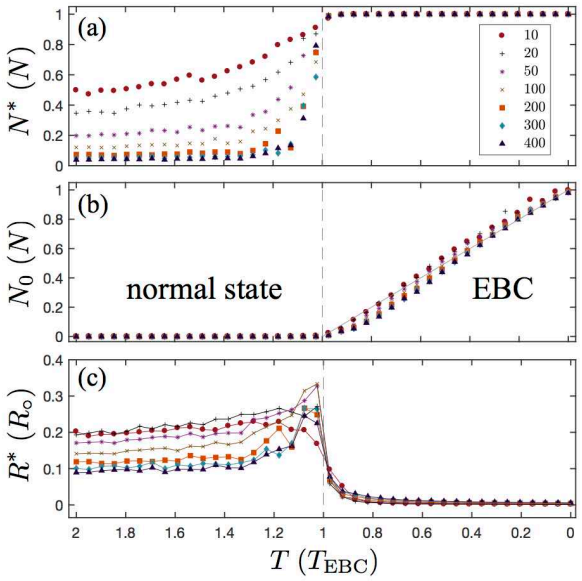

FIG. 2. (color online) Fraction of vortices in the largest cluster (a), the EBC fraction, Eq. (6), (b) and the mean cluster radius $R^* = \text{Std}(r_j)$, where $\mathbf{r}_j$ is the vector of positions of the vortices in the largest cluster (c) as functions of scaled temperature. Data is shown for systems with different vortex numbers as indicated in the legend. The function $1-T/T_{\rm EBC}$, where $T_{\rm EBC} = -0.25\alpha N_{\rm tot}$, is shown as a solid line in (b) for $|T| < |T_{\rm EBC}|$ and the vertical dashed line marks the critical point. All quantities are ensemble averaged.

Figure 1 (a) shows a vortex configuration at a high negative temperature $T = 10^6\ T_{\rm EBC}$ revealing a fairly disordered configuration of vortices with an abundance of vortex dipoles and small clusters. Figure 1 (b) shows a vortex configuration at $T = 1.022\ T_{\rm EBC}$ just above the critical EBC transition temperature. Note how nearly all the vortices have already clustered into two Onsager vortices although the EBC fraction remains zero. This clearly shows that vortex clustering precedes the condensation and that the presence of Onsager vortices is not a sufficient criterion for the existence of an EBC of Onsager vortices in the system. Figure 1 (c) shows Onsager vortices at temperature $T = 0.778\ T_{\rm EBC}$ where the system has an EBC fraction of ≈ 0.1. The qualitative similarity between the stream lines in Figs 1 (b) and (c) is striking despite the states lying on different sides of the transition. Notwithstanding the rapid growth of the vortex dipole moment, the EBC transition does not involve a breaking of a continuous rotation symmetry of the vortex configuration. In this sense the EBC transition behaves similarly to the non-symmetry-breaking BKT phase transition [12–14, 40, 41, 50–54]. The illusion of a spontaneous symmetry breaking is a relic due to the presence of two vortex species, both of which form a separate EBC. The EBC transition occurs even in a maximally imbalanced case where only one type of vortices is present in the system in which case the dipole moment is identically zero at all temperatures. In the general imbalanced case with N_+

vortices and N_- antivortices with $N_{\rm tot} = N_+ + N_-$ there are two critical temperatures. When the temperature approaches negative zero, the majority species condenses first at $T_{\rm EBC} = -\alpha N_{\rm maj}/2$, followed by the condensation of the minority species at $T_{\rm EBC} \approx -\alpha N_{\rm min}/2$, where the latter is shifted slightly toward negative zero due to the interaction with the condensate of the majority species.

Figure 2 is our main result showing (a) the largest cluster fraction, (b) the EBC fraction, and (c) the mean radius of the largest cluster in the system as functions of temperature in units of the EBC critical temperature $T_{\rm EBC} = -0.25\alpha N_{\rm tot}$. As mentioned previously, Fig. 2 reveals that the system becomes completely clustered before the EBC critical point is reached. The largest cluster fraction Fig. 2(a) is strongly dependent on the total number of vortices in the system. In contrast, the EBC fraction, shown in Fig. 2(b), remains zero at all temperatures $|T| > |T_{\rm EBC}|$ and thereafter increases as the absolute negative zero is approached. Figure 2(c) shows the mean radii of the largest vortex clusters as functions of temperature. As the critical temperature is approached from the disordered side, the largest cluster tends to grow in size as ever more vortices are joining in. In the condensed phase the cluster rapidly shrinks as the phase-space density, and hence the condensate fraction, increases. Importantly, the condensate fraction shows universality in the sense that it is consistent with data collapsing onto a single curve, indicating the EBC fraction becoming a vortex number independent quantity in the large vortex number limit. This is consistent both with the data in Fig. 2(b) and the non-interacting vortex particle model mapped onto a one-dimensional non-interacting Bose gas. In atomic BECs particle interactions may reduce the condensate fraction with respect to the non-interacting case, particularly in the vicinity of the critical temperature. Similarly, the long-range vortex interactions may be responsible for the non-linear behaviour of the EBC condensate fraction near the critical point.

With the ability to quantify the Einstein–Bose condensation of Onsager vortices, we have revisited the dynamical mean-field simulations of Ref. [28]. Figure 3 shows a typical result revealing that in this neutral vortex system, the largest cluster fraction and vortex dipole moment are practically equivalent observables. However, although the system is continually evaporatively heated, the condensate fraction remains zero for all times. The initial vortex number in this simulation is 100 and it decays to the final value of 12. Comparing the largest cluster fraction in Fig. 3 with Fig. 2(a) shows that this system is initially at temperature $|T| \gg |T_{\rm EBC}|$ and evaporatively heats reaching a final temperature of $|T| \gtrsim |T_{\rm EBC}|$. However, once the system becomes fully clustered and is at the verge of the EBC transition, the evaporative heating mechanism switches off [9] and the Einstein–Bose condensation is unable to proceed.

In conclusion, we have employed a vortex–particle duality to establish a correspondence between vortices in a two-dimensional fluid and a one-dimensional gas of vortex particles. We have used this mapping to provide a quantitative definition for an Einstein–Bose condensate fraction of Onsager vortices and used this to show the clear difference between a condensate of Onsager vortices and a quasi-condensate of vortex clusters. Furthermore, we have shown that the evaporative heating of vortices does not lead to the crossing of the EBC critical point. In steady-state two-dimensional incompressible fluid turbulence the inverse energy cascade of the Kraichnan model predicts a spectral power-law kinetic energy spectrum. However, once large Onsager vortices form in the system, the energy spectrum changes drastically and would no longer be consistent with the structure of the inverse energy cascade. In particular, the system scale Onsager vortices that form before they can condense facilitate energy transport across all spatial scales in the system. Hence, we postulate that even the inverse energy cascade mechanism of driven classical two-dimensional turbulence may not supply sufficient amount of energy for condensation and that instead a direct forcing at the Onsager vortex scale may be required to realise the Einstein–Bose condensation of Onsager vortices. Ultimately, deep in the EBC phase a phase-space Wigner crystallisation of vortices with hard cores takes place [9] while true point vortices would condense into multiply quantised vortices [55]. An interesting future direction is to investigate if an understanding of such strongly correlated vortex systems can be developed on the basis of the theory of Tonks-Girardeau gas.

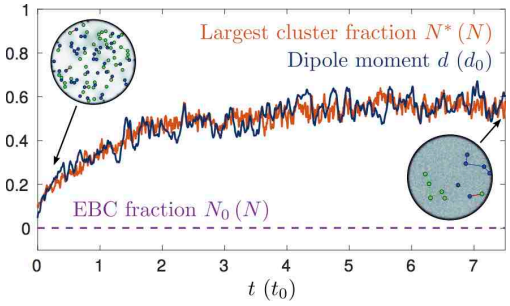

FIG. 3. (color online) Vortex dipole moment (solid blue) expressed in units of $d_0 = \kappa R_\circ N$, largest cluster fraction (solid orange) and EBC condensate fraction (dashed purple) as functions of time calculated from a dynamical mean-field simulation. The unit of time is $t_0 = \hbar/\mu$, where μ is the chemical potential. The initial vortex number is 100 and as the system evaporatively heats up, the vortex number decays to a value of 12 at the end of the simulation, see Ref. [28] for details.

ACKNOWLEDGMENTS

We acknowledge support from an Australian Postgraduate Award (A.G.), the Australian Research Council via Discovery Project No. DP130102321 and DP170104180

(T.S.), and the nVidia Hardware Grant Program. This research was undertaken with the assistance of resources from the National Computational Infrastructure (NCI), which is supported by the Australian Government.

[1] L. Onsager, Il Nuovo Cimento Series 9 **6**, 279 (1949), ISSN 0029-6341.
[2] G. L. Eyink and K. R. Sreenivasan, Rev. Mod. Phys. **78**, 87 (2006).
[3] E. M. Purcell and R. V. Pound, Phys. Rev. **81**, 279 (1951).
[4] A. S. Oja and O. V. Lounasmaa, Rev. Mod. Phys. **69**, 1 (1997).
[5] S. Braun, J. P. Ronzheimer, M. Schreiber, S. S. Hodgman, T. Rom, I. Bloch, and U. Schneider, Science **339**, 52 (2013), ISSN 0036-8075.
[6] R. H. Kraichnan, Physics of Fluids **10**, 1417 (1967).
[7] R. H. Kraichnan and D. Montgomery, Reports on Progress in Physics **43**, 547 (1980).
[8] J. A. Viecelli, Physics of Fluids **7**, 1402 (1995).
[9] T. Simula, M. J. Davis, and K. Helmerson, Physical Review Letters **113**, 165302 (2014).
[10] A. M. Salzberg and S. Prager, J. Chem. Phys. **38**, 2587 (1963).
[11] E. H. Hauge and P. C. Hemmer, Phys. Norv. **5**, 209 (1971).
[12] V. L. Berezinskii, Sov. Phys. JETP **32**, 493 (1971).
[13] V. L. Berezinskii, Sov. Phys. JETP **34**, 610 (1972).
[14] J. M. Kosterlitz and D. J. Thouless, J. Phys. **C6**, 1181 (1973).
[15] T. W. Neely, E. C. Samson, A. S. Bradley, M. J. Davis, and B. P. Anderson, Phys. Rev. Lett. **104**, 160401 (2010).
[16] R. Navarro, R. Carretero-González, P. J. Torres, P. G. Kevrekidis, D. J. Frantzeskakis, M. W. Ray, E. Altuntaş, and D. S. Hall, Phys. Rev. Lett. **110**, 225301 (2013).
[17] E. A. L. Henn, J. A. Seman, G. Roati, K. M. F. Magalhães, and V. S. Bagnato, Phys. Rev. Lett. **103**, 045301 (2009).
[18] T. W. Neely, A. S. Bradley, E. C. Samson, S. J. Rooney, E. M. Wright, K. J. H. Law, R. Carretero-González, P. G. Kevrekidis, M. J. Davis, and B. P. Anderson, Phys. Rev. Lett. **111**, 235301 (2013).
[19] W. J. Kwon, G. Moon, J. Y. Choi, S. W. Seo, and Y. I. Shin, Phys. Rev. A **90**, 063627 (2014).
[20] W. J. Kwon, J. H. Kim, S. W. Seo, and Y. I. Shin, ArXiv e-prints (2016), 1608.02762.
[21] S. W. Seo, B. Ko, J. H. Kim, and Y.-i. Shin, ArXiv e-prints (2016), 1610.06635.
[22] K. Henderson, C. Ryu, C. MacCormick, and M. G. Boshier, New Journal of Physics **11**, 043030 (2009).
[23] A. L. Gaunt, T. F. Schmidutz, I. Gotlibovych, R. P. Smith, and Z. Hadzibabic, Phys. Rev. Lett. **110**, 200406 (2013).
[24] L. Chomaz, L. Corman, T. Bienaimé, R. Desbuquois, C. Weitenberg, S. Nascimbène, J. Beugnon, and J. Dalibard, Nature Communications **6**, 6162 (2015), 1411.3577.
[25] T. A. Bell, J. A. P. Glidden, L. Humbert, M. W. J. Bromley, S. A. Haine, M. J. Davis, T. W. Neely, M. A. Baker, and H. Rubinsztein-Dunlop, New Journal of Physics **18**, 035003 (2016).
[26] J. Lee, S. Eckel, F. Jendrzejewski, C. J. Lobb, G. K. Campbell, and W. T. Hill, III, ArXiv e-prints (2015), 1506.08413.
[27] G. Gauthier, I. Lenton, N. McKay Parry, M. Baker, M. J. Davis, H. Rubinsztein-Dunlop, and T. W. Neely, ArXiv e-prints (2016), 1605.04928.
[28] A. J. Groszek, T. P. Simula, D. M. Paganin, and K. Helmerson, Phys. Rev. A **93**, 043614 (2016).
[29] G. W. Stagg, A. J. Allen, N. G. Parker, and C. F. Barenghi, Phys. Rev. A **91**, 013612 (2015).
[30] A. C. White, C. F. Barenghi, and N. P. Proukakis, Phys. Rev. A **86**, 013635 (2012).
[31] M. T. Reeves, T. P. Billam, B. P. Anderson, and A. S. Bradley, Phys. Rev. Lett. **110**, 104501 (2013).
[32] T. P. Billam, M. T. Reeves, B. P. Anderson, and A. S. Bradley, Phys. Rev. Lett. **112**, 145301 (2014).
[33] M. T. Reeves, T. P. Billam, B. P. Anderson, and A. S. Bradley, Phys. Rev. Lett. **114**, 155302 (2015).
[34] A. Skaugen and L. Angheluta, Phys. Rev. E **93**, 032106 (2016).
[35] X. Yu, T. P. Billam, J. Nian, M. T. Reeves, and A. S. Bradley, Phys. Rev. A **94**, 023602 (2016).
[36] A. Skaugen and L. Angheluta, ArXiv e-prints (2016), 1610.04382.
[37] Y. Yatsuyanagi, Y. Kiwamoto, H. Tomita, M. M. Sano, T. Yoshida, and T. Ebisuzaki, Phys. Rev. Lett. **94**, 054502 (2005).
[38] See Supplemental Material at [URL will be inserted by publisher] for the details of the vortex classification algoritm.
[39] Y. Kagan, V. A. Kashurnikov, A. V. Krasavin, N. V. Prokof'ev, and B. V. Svistunov, Phys. Rev. A **61**, 043608 (2000).
[40] Z. Hadzibabic, P. Krüger, M. Cheneau, B. Battelier, and J. Dalibard, Nature (London) **441**, 1118 (2006).
[41] P. Cladé, C. Ryu, A. Ramanathan, K. Helmerson, and W. D. Phillips, Physical Review Letters **102**, 170401 (2009), 0805.3519.
[42] C.-L. Hung, X. Zhang, N. Gemelke, and C. Chin, Nature (London) **470**, 236 (2011), 1009.0016.
[43] Y. B. Pointin and T. S. Lundgren, Physics of Fluids **19** (1976).
[44] J. B. Keller, Annals of Physics **4**, 180 (1958).
[45] W. Ketterle and N. J. van Druten, Phys. Rev. A **54**, 656 (1996).
[46] S. M. M. Virtanen, T. P. Simula, and M. M. Salomaa, Phys. Rev. Lett. **86**, 2704 (2001).
[47] V. Bagnato and D. Kleppner, Phys. Rev. A **44**, 7439 (1991).
[48] N. R. Cooper, Advances in Physics **57**, 539 (2008), 0810.4398.
[49] A. L. Fetter, Reviews of Modern Physics **81**, 647 (2009).
[50] N. Prokof'ev, O. Ruebenacker, and B. Svistunov, Phys. Rev. Lett. **87**, 270402 (2001).
[51] T. P. Simula and P. B. Blakie, Phys. Rev. Lett. **96**, 020404 (2006).
[52] T. P. Simula, M. J. Davis, and P. B. Blakie, Phys. Rev. A **77**, 023618 (2008).

[53] R. N. Bisset, M. J. Davis, T. P. Simula, and P. B. Blakie, Phys. Rev. A **79**, 033626 (2009).
[54] J. V. José, *40 Years of Berezinskii-Kosterlitz-Thouless Theory* (World Scientific Publishing Co, 2013).
[55] T. P. Simula, S. M. M. Virtanen, and M. M. Salomaa, Phys. Rev. A **65**, 033614 (2002).

Supplementary Material for: Einstein–Bose Condensation of Onsager Vortices

Rahil N. Valani[1,2], Andrew J. Groszek[1], Tapio P. Simula[1]
[1]*School of Physics and Astronomy, Monash University, Victoria 3800, Australia and*
[2]*Department of Mechanical and Aerospace Engineering, Monash University, Victoria 3800, Australia*

I. VORTEX CLASSIFICATION ALGORITHM

We assign each vortex in a given configuration of N vortices a unique and arbitrarily chosen label from the set $\{v_1, v_2, \ldots, v_N\}$. The vortex configuration is then described by a corresponding set of positions $\{z_1, z_2, \ldots, z_N\}$ (in two-dimensional complex coordinates, where $z_j = x_j + iy_j$) and circulation signs $\{s_1, s_2, \ldots, s_N\}$, which here take the value $s_j = \pm 1$, denoting clockwise or anti-clockwise circulation. The algorithm does not prioritise any vortex and yields the same classification outcome regardless of the choice of vortex labelling. Figure 1 shows an example configuration of twelve judiciously numbered point vortices. The vortex classification algorithm is outlined below.

A. Step 1: Find dipole and cluster candidates

For each vortex v_j, we locate the nearest opposite sign (NOS) vortex and label it as $(v_{\rm NOS})_j$ [*i.e.* the nearest vortex which satisfies $s_j(s_{\rm NOS})_j < 0$]. We define the distance to this vortex to be $(R_{\rm NOS})_j \equiv |z_j - (z_{\rm NOS})_j|$. We then check to see if any other vortices (which are same-sign, by necessity) fall within the disk of radius $R_{\rm NOS}$ centered at vortex v_j.

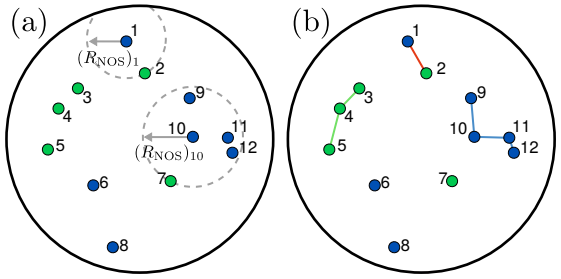

FIG. 1. A configuration of twelve point vortices, (a) before and (b) after the classification algorithm has been applied. Vortices are drawn in blue, while antivortices are drawn in green. In panel (a), dashed circles are drawn centered on v_1 and v_{10}, denoting the respective distances $(R_{\rm NOS})_j$ to the nearest opposite signed vortex. Because v_2 is the closest vortex to v_1 and is of opposite sign, v_2 is labelled as a dipole candidate for v_1. Vortex v_{10}, on the other hand, is closer to v_9, v_{11} and v_{12} than it is to v_7; hence, these three vortices become cluster candidates for v_{10}. The lines joining clustered vortices in (b) are drawn using a minimum spanning tree algorithm, which is applied once all vortices have been labelled into the sets of clusters, dipoles or free vortices.

(i) *Dipoles:* If not, then $(v_{\rm NOS})_j$ is labelled as a dipole candidate for v_j [*e.g.* in Fig. 1(a), v_2 is labelled as a dipole candidate for v_1].

(ii) *Clusters:* If there are $n_j \geq 1$ vortices which are nearer to v_j than $(v_{\rm NOS})_j$, then these are labelled as cluster candidates for v_j [*e.g.* vortex v_{10} in Fig. 1(a), for which v_9, v_{11} and v_{12} are cluster candidates].

Each vortex v_j now has a corresponding set of candidate vortex labels, which we denote by $\mathbf{l}_j$. For case (i), $\mathbf{l}_j$ consists of a single opposite sign vortex, which is a dipole candidate. For case (ii), $\mathbf{l}_j$ is a list of n_j same-sign cluster candidates.

Table I below displays the lists $\mathbf{l}_j$ that are constructed in Step 1 of the algorithm when it is applied to the configuration shown in Fig. 1.

TABLE I. Collation of $\mathbf{l}_j$ lists for the configuration shown in Fig. 1 after dipole and cluster candidates have been identified. Each row corresponds to a particular vortex v_j (leftmost column) and the list of all other vortices, ordered from left to right in increasing distance from v_j. Vortices/antivortices v_k are denoted with blue/green font if $|z_j - z_k| \leq (R_{\rm NOS})_j$. All vortices for which $|z_j - z_k| > (R_{\rm NOS})_j$ are colored in gray, as these cannot be dipole or cluster candidates. The lists $\mathbf{l}_j$ consist of either a single opposite sign vortex (*e.g.* row 1, corresponding to vortex v_1, which has $\mathbf{l}_1 = \{v_2\}$), or a set of ≥ 1 same-sign vortices (*e.g.* row 4, corresponding to vortex v_4, for which $\mathbf{l}_4 = \{v_3, v_5\}$).

v_j	$\mathbf{l}_j$										
$\mathbf{v_1}$	$\mathbf{v_2}$	v_3	v_9	v_4	v_{10}	v_5	v_{11}	v_7	v_6	v_{12}	v_8
$\mathbf{v_2}$	$\mathbf{v_1}$	v_9	v_3	v_{10}	v_4	v_{11}	v_7	v_{12}	v_5	v_6	v_8
$\mathbf{v_3}$	$\mathbf{v_4}$	$\mathbf{v_1}$	v_2	v_5	v_6	v_9	v_{10}	v_7	v_{11}	v_8	v_{12}
$\mathbf{v_4}$	$\mathbf{v_3}$	$\mathbf{v_5}$	$\mathbf{v_6}$	v_2	v_1	v_9	v_7	v_{10}	v_8	v_{11}	v_{12}
$\mathbf{v_5}$	$\mathbf{v_4}$	$\mathbf{v_6}$	v_3	v_8	v_2	v_7	v_1	v_{10}	v_9	v_{11}	v_{12}
$\mathbf{v_6}$	$\mathbf{v_5}$	v_8	v_7	v_4	v_3	v_{10}	v_2	v_9	v_{12}	v_{11}	v_1
$\mathbf{v_7}$	$\mathbf{v_{10}}$	v_{12}	v_{11}	v_6	v_9	v_8	v_2	v_5	v_3	v_4	v_1
$\mathbf{v_8}$	$\mathbf{v_6}$	$\mathbf{v_7}$	v_5	v_{10}	v_4	v_{12}	v_{11}	v_3	v_9	v_2	v_1
$\mathbf{v_9}$	$\mathbf{v_{10}}$	$\mathbf{v_2}$	v_{11}	v_{12}	v_7	v_1	v_3	v_4	v_6	v_5	v_8
$\mathbf{v_{10}}$	$\mathbf{v_{11}}$	$\mathbf{v_9}$	$\mathbf{v_{12}}$	$\mathbf{v_7}$	v_2	v_6	v_1	v_3	v_8	v_4	v_5
$\mathbf{v_{11}}$	$\mathbf{v_{12}}$	$\mathbf{v_{10}}$	$\mathbf{v_9}$	$\mathbf{v_7}$	v_2	v_1	v_6	v_3	v_8	v_4	v_5
$\mathbf{v_{12}}$	$\mathbf{v_{11}}$	$\mathbf{v_{10}}$	$\mathbf{v_7}$	v_9	v_2	v_6	v_8	v_1	v_3	v_4	v_5

B. Step 2: Find mutually agreeing candidates

In the second step of the algorithm, the lists $\mathbf{l}_j$ are checked sequentially for mutual members. This process

is shown schematically in Fig. 2 for the example configuration shown in Fig. 1 and Table I.

(i) *Dipoles:* If a list $\mathbf{l}_j$ consists of a single dipole candidate v_k, then the list $\mathbf{l}_k$ is checked to see if it contains (only) the vortex v_j. If so, then the two vortices are mutual nearest neighbours of opposite sign, and are classified as a dipole (*e.g.* vortices v_1 and v_2 in Fig. 2). If not, then the vortices are left unclassified (*e.g.* vortices v_6 and v_5 in Fig. 2).

(ii) *Clusters:* If a list $\mathbf{l}_j$ consists of a set of cluster candidate vortices $\{v_k\}$, then the lists $\{\mathbf{l}_k\}$ are all checked to see if they contain the vortex v_j. For each list $\mathbf{l}_k$ that does contain v_j, the two vortices v_j and v_k are labelled as belonging to the same cluster (*e.g.* in Fig. 2, vortex v_4 "checks" both $\mathbf{l}_3$ and $\mathbf{l}_5$ to see if it is a member of either. It is found to be a member of both, so all three vortices are placed in a single cluster). For each list $\mathbf{l}_k$ that does not contain v_j, neither vortex label is updated (*e.g.* vortex v_7 and v_{10} in Fig. 2). Note that not all members of a single cluster have to be mutual candidates of one another. In the example shown in Fig. 2, v_9 is only a mutual neighbour with v_{10}, but is still placed in the same cluster as v_{11} and v_{12}. As the algorithm proceeds, vortices may be assigned to existing clusters, or previously classified clusters may become merged.

Any vortices left unclassified after this process are classified as free vortices, as they have no mutual dipole or cluster neighbours (*e.g.* vortex v_6 in Fig. 2).

In Fig. 2(b), any two vortices that are connected by a two-directional link are part of the same cluster or dipole,

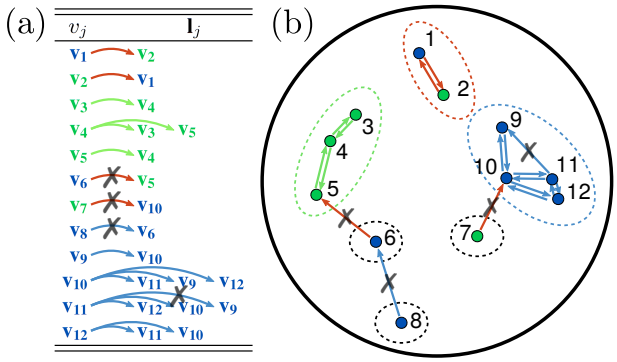

FIG. 2. The process of identifying mutual neighbours, shown equivalently as (a) a table of candidate lists $\mathbf{l}_j$ taken from Table I, and (b) drawn directly onto the example vortex configuration from Fig. 1. An arrow is drawn from each vortex v_j to all the members of its candidate list $\mathbf{l}_j$. Only when arrows point in both directions between v_j and v_k are they defined to be mutual neighbours. All arrows that are one-directional have been crossed out in both panels. In panel (b), dashed circles are drawn around clusters (blue/green for positive/negative), dipoles (red) and free vortices (black).

while any vortex that has no two-directional links is a free vortex.

To reduce computation, the checking of mutual candidates can be restricted such that it is only initiated for v_j and v_k if $j > k$. Alternatively, once a pair of vortices has been checked, then v_j could be removed from $\mathbf{l}_k$ and vice versa.